Two Families of Centered Zirconium Cluster Phases with $M_{1,2}M'Cl_6{\cdot}Zr_6Cl_{12}Z$ Compositions

Jie Zhang and John D. Corbett*

Department of Chemistry, Iowa State University, Ames, Iowa 50011

Received October 6, 1992

New examples of the $K_2Zr_7Cl_{18}H$ ($R\bar{3}$) structure were established for seven $M_2M'Zr_6Cl_{18}Z$ and five (defect) $MM'Zr_6Cl_{18}Z$ examples with appropriate combinations of M = K–Cs, M' = Ca, Ba, La, and Z = B, C, Mn, Fe, all with closed-shell (14- or 18-electron) clusters. New $CsLuNb_6Cl_{18}$-type ($P\bar{3}1c$) members were found for $CsLaZr_6Cl_{18}$(C or Fe) and $RbLaZr_6Cl_{18}Fe$. Single-crystal X-ray studies were carried out for $(K_{0.85}Ba_{0.13})BaZr_6Cl_{18}C$ ($R\bar{3}$, Z = 3, a = 9.8697 (2) Å, c = 27.653 (4) Å, R/R_w = 1.5/2.3% for 1748 independent data) and $CsLaZr_6Cl_{18}Fe$ ($P\bar{3}1c$, Z = 2, a = 9.6404 (4) Å, c = 18.332 (1) Å, R/R_w = 3.0/4.2% for 957 data). The rhombohedral $CsLaZr_6Cl_{18}$(C or Fe) and $RbLaZr_6Cl_{18}Fe$ phases were never obtained free of their $P\bar{3}1c$ polymorphs. Systematic studies showed that a conventional phase transition was not responsible, rather a irreversible conversion to the trigonal phase on a time scale of weeks at 700–900 °C. The two structures, factors in their stabilities and interconversion, and their relationship to $Ba_3Zr_6Cl_{18}Be$ are described and discussed.

Introduction

Synthetic ventures guided by a knowledge of electronic and structural principles have led to the discovery of an extremely large collection of zirconium chloride cluster phases, generally with the generic formula $M^I_x[Zr_6Cl_{12}Z]Cl_n$ ($0 \le x, n \le 6$) where Z centers the Zr_6Cl_{12} cluster units.[1-5] A common feature of all examples are cluster electron counts of, or close to (±1), the optimal values of 14 for Z = H, Be, B, C, N and 18 for Z = Mn, Fe, Co, Ni. In spite of this electronic constraint, the groups exhibit a wide variety of structure types with intriguing structural interrelationships. Part of the versatility is afforded by the interstitial elements Z and by the nature of the cluster networks that are defined by the value of n, but the types and number of countercations M incorporated into the lattice are also significant factors in determining cluster formation, structure, and stability. The cation effects are best illustrated for the end members of the series $M_xZr_6Cl_{18}Z$ (n = 6), where direct cluster connections no longer exist and the cluster–countercation interactions become dominant in the structure determination.

Niobium and zirconium form all five distinctive $M_x(Zr,Nb)_6Cl_{18}(Z)$ structure types that have isolated cluster units in them, namely, $Li_6Zr_6Cl_{18}H$,[4] $Rb_5Zr_6Cl_{18}B$,[2] $K_4Nb_6Cl_{18}$,[6] $K_2Zr_7Cl_{18}H$,[7] and $CsLuNb_6Cl_{18}$.[8] The first three have only alkali metals as the countercations, and relatively large cation:cluster ratios are required for stability. On the other hand, the last two incorporate an additional polyvalent cation M' in addition to alkali metal M, so that a formal $M'Cl_6$ anion in each acts as a bridge with its chlorine atoms also bonded exo to vertices in six separate clusters. Thus $K_2Zr_7Cl_{18}(H)$, among the first zirconium chloride cluster phases discovered, can equally well be described as the double salt $K_2ZrCl_6{\cdot}Zr_6Cl_{12}H$. Several other zirconium cluster phases with this $R\bar{3}$ structure have since been found with other alkali metals and Z = H or Be,[9] and a family of ternary or quaternary niobium (and some tantalum) cluster phases $M_xM'Nb_6Cl_{18}$ (M' = rare-earth metal, x = 0–2)[10,11] were later recognized to have the $K_2Zr_7Cl_{18}H$ structure or a defect version of it as well.[12,13] The recently discovered $Ba_3Zr_6Cl_{18}Be$ with M = M' has a superstructure of this double salt ($R\bar{3}c$).[14] The $CsLuNb_6Cl_{18}$ [$=(CsLuCl_6^{2-})Nb_6Cl_{12}^{2+}$] structure type ($P\bar{3}1c$) is closely related to the original double salt for x = 1, and both types were observed to coexist at intermediate temperatures in niobium chloride cluster systems for M = Rb and M' = La, Ce.[13] However, the nature of the apparent transition was not defined.

Our search for new cluster phases with related structures originated with a desire to expand the diversity of cluster compositions. Selection of the proper combination of countercations and interstitial atoms was found to afford numerous new examples of $M_xM'Zr_6Cl_{18}Z$ compositions with M = K–Cs, M' = Ca, Ba, La, Z = B, C, Mn, Fe, and x = 1, 2 in the $K_2Zr_7Cl_{18}H$ or $CsLuNb_6Cl_{18}$ structures. These compounds exhibit fascinating interrelationships, and they also afford the opportunity to explore reasons for the phase transition between the two noted above.

Experimental Section

The quality of the reactor-grade zirconium metal, the preparations of $ZrCl_4$ and powdered zirconium, the reaction techniques utilizing welded tantalum containers, and the Guinier powder diffraction and calculational methods have been described before.[15] The sources of interstitial atoms were the elements C (Union Carbide, spectroscopic grade) or B (AESAR, amorphous, <1 μm) or the metal chlorides obtained through dehydration of $MnCl_2{\cdot}4H_2O$ (Baker, analyzed reagent) with $SOCl_2$ or slow heating of $FeCl_3$ (ROC/RIC, 99%) under high vacuum followed by vacuum sublimation of the chlorides. For some reactions, Fe powder (Baker, analyzed reagent) was employed instead, without any noticeable alteration of the end products or the yield. The alkali-metal chlorides KCl, RbCl, and CsCl were dried under high vacuum and sublimed prior to use, while $BaCl_2$ and $CaCl_2$ were obtained by slow thermal decomposition of the hydrates under high vacuum (and checked by powder pattern). $LaCl_3$ was prepared through reaction of La_2O_3 with NH_4Cl followed by multiple sublimations of the crude product at 800 °C in Ta containers under dynamic vacuum. The phase purities of the starting materials were established with the aid of Guinier powder patterns when necessary, and all reactants and products were handled only in a glovebox filled with dry nitrogen.

(1) Ziebarth, R. P.; Corbett, J. D. *Acc. Chem. Res.* **1989**, *22*, 256.
(2) Ziebarth, R. P.; Corbett, J. D. *J. Am. Chem. Soc.* **1989**, *111*, 3272.
(3) Zhang, J.; Corbett, J. D. *Inorg. Chem.* **1991**, *30*, 431.
(4) Zhang, J.; Ziebarth, R. P.; Corbett, J. D. *Inorg. Chem.* **1992**, *31*, 614.
(5) Corbett, J. D. In *Modern Perspectives in Inorganic Crystal Chemistry*; Parthé, E., Ed.; NATO ASI Series C; Kluwer Academic Publishers: Dordrecht, The Netherlands, 1992; pp 27–56.
(6) Simon, A.; von Schnering, H.-G.; Schäfer, H. *Z. Anorg. Allg. Chem.* **1968**, *361*, 235.
(7) Imoto, H.; Corbett, J. D.; Cisar, A. *Inorg. Chem.* **1981**, *20*, 145.
(8) Ihmaine, S.; Perrin, C.; Sergent, M. *Acta Crystallogr.* **1989**, *C45*, 705.
(9) Ziebarth, R. P.; Corbett, J. D. *J. Solid State Chem.* **1989**, *80*, 56.
(10) Ihmaine, S.; Perrin, C.; Sergent, M. *C. R. Acad. Sci. (Paris)* **1986**, *303*, 1293.
(11) Ihmaine, S.; Perrin, C.; Sergent, M. *Acta Crystallogr.* **1987**, *C43*, 813.
(12) Ihmaine, S.; Perrin, C.; Pena, O.; Sergent, M. *J. Less-Common Met.* **1988**, *137*, 323.
(13) Perrin, C.; Ihmaine, S.; Sergent, M. *New J. Chem.* **1988**, *137*, 21.
(14) Zhang, J.; Corbett, J. D. *Z. Anorg. Allg. Chem.* **1991**, *598/599*, 363.
(15) Ziebarth, R. P.; Corbett, J. D. *J. Am. Chem. Soc.* **1987**, *109*, 4844.

0020-1669/93/1332-1566$04.00/0

Table I. Unit Cell Parameters[a] (Å) and Volumes (Å^3) for New $K_2ZrCl_6{\cdot}Zr_6Cl_{12}H$-Type ($R\bar{3}$) and $CsLuNb_6Cl_{15}$-Type ($P\bar{3}1c$) Compounds

compound	a	c	V
	$K_2Zr_7Cl_{18}(H)$ Type		
$K_2LaZr_6Cl_{18}B$	9.5749(9)	26.661(5)	2116.8(5)
$KLaZr_6Cl_{18}C$	9.538(2)	26.549(5)	2091.7(8)
$Cs_2LaZr_6Cl_{18}Mn$	9.7996(5)	27.296(3)	2270.1(3)
$KCsLaZr_6Cl_{18}Mn$	9.7478(9)	27.210(3)	2239.1(5)
$KLaZr_6Cl_{18}Fe$	9.703(3)	26.88(1)	2191(2)
$CsLaZr_6Cl_{18}Fe$[b]	9.746(2)	27.197(7)	2237.3(9)
$(K + Ba)_2BaZr_6Cl_{18}C$[c]	9.5950(4)	26.926(2)	2146.8(3)
$Cs_2CaZr_6Cl_{18}Fe$	9.6890(4)	27.113(2)	2204.3(3)
$KCsCaZr_6Cl_{18}Fe$	9.6335(6)	27.013(2)	2171.1(3)
$(Cs + Ba)_2BaZr_6Cl_{18}Fe$[d]	9.8697(2)	27.653(4)	2332.8(5)
	$CsLuNb_6Cl_{18}$ Type		
$CsLaZr_6Cl_{18}Fe$	9.6404(4)	18.332(1)	1475.5(2)
$RbLaZr_6Cl_{18}Fe$	9.6229(9)	18.262(3)	1464.5(4)
$CsLaZr_6Cl_{18}C$	9.5098(9)	17.939(3)	1405.0(3)

[a] All values are from Guinier powder diffraction data. [b] Coexists with the $P\bar{3}1c$ phase. See text. [c] The refined stoichiometry is (K_xBa_y)-$BaZr_6Cl_{18}C$ with $x = 0.85(9)$, $y = 0.13(3)$. [d] Amount of minor Ba in M site is unknown.

Table II. Selected Crystal Data[a]

composition	$(K + Ba)_2BaZr_6Cl_{18}C$	$CsLaZr_6Cl_{18}Fe$
space group, Z	$R\bar{3}$ (No. 148), 3	$P\bar{3}1c$ (No. 163), 2
crystal dimens, mm	0.40 × 0.14 × 0.12	0.20 × 0.12 × 0.10
abs coeff μ, cm^{-1} (Mo Kα)	54.1	67.5
range of transm coeff	0.80–1.00	0.70–1.00
R,[b] %	1.5	3.0
R_w,[c] %	2.3	4.2

[a] Cell parameters in Table I. [b] $R = \sum||F_o| - |F_c||/\sum|F_o|$. [c] $R_w = [\sum w(|F_o| - |F_c|)^2/\sum w(F_o)^2]^{1/2}$; $w = \sigma_F^{-2}$.

Syntheses. New phases obtained with the $K_2Zr_7Cl_{18}Z$ ($R\bar{3}$) and $CsLuNb_6Cl_{18}$ ($P\bar{3}1c$) type structures are listed in Table I. ($R\bar{3}$ structures for $RbLaZr_6Cl_{18}Fe$ and $CsLaZr_6Cl_{18}C$ were also seen as minor components—see Results and Discussion.) The compounds containing Ca^{2+} or La^{3+} were obtained by design. In contrast, $(K+Ba)_2BaZr_6Cl_{18}C$ and $(Cs+Ba)_2BaZr_6Cl_{18}Fe$ were discovered following reactions aimed at the stoichiometric syntheses of hypothetical $MBaZr_6Cl_{17}Z$ (M = K, Cs; Z = C, Fe) with 14- or 18-electron clusters in structures related to Ba_2-$Zr_6Cl_{17}B$,[16] so that small amounts of $BaCl_2$ and $Zr_6Cl_{14}Z$ were also present in the products. The majority of the reactions were run at 800–850 °C for 15–20 days, and then the reaction mixtures were rapidly cooled by removing the containers from the tube furnaces. Especially prolonged heating periods of up to 70 days were employed for certain systems to investigate the transformation between the two structure types. The structure type of each product was established by comparison of observed and calculated X-ray powder patterns. The new $M_xM'Zr_6Cl_{18}Z$ compounds can be produced in high yield (>95%, viz., as single-phase products as judged by Guinier powder diffraction patterns) when loaded for the correct overall compositions, except for the special cases with M = Rb, Cs, Z = C, Fe, and $x = 1$, where a mixture of both structure types was often obtained in high total yield. However, adequate monocrystals of trigonal $CsLaZr_6Cl_{18}Fe$ were not readily obtained in this way. Therefore, a reaction with this stoichiometry was heated in a 800/900 °C temperature gradient for 50 days. Because of the relatively high temperature and large gradient, the yield of cluster phases (estimated on the basis of the powder pattern) was only about 30%, the rest of the products being ZrCl, $ZrCl_4$, $LaCl_3$, and an unidentified phase. The major cluster product was crystals of $CsLaZr_6Cl_{18}Fe$ in the $R\bar{3}$ structure.

Structure Determinations. $(K+Ba)_2BaZr_6Cl_{18}C$. A deep red, transparent, gemlike crystal was indexed on the diffractometer with a rhombohedral cell, in agreement with the powder pattern determination that the main product was isostructural with $K_2Zr_7Cl_{18}H$ ($R\bar{3}$).[7] A full structure analysis was carried out to determine the chemical composition and to verify that the M′ position was occupied by barium. Diffraction data were collected over one hemisphere at room temperature with the aid of a RIGAKU diffractometer after the unit cell, its Laue symmetry, and the setting were confirmed by axial photographs and the Laue program. Some other data are listed in Table II.

No decay correction was necessary, a 3% intensity increase for the standard reflections presumably being caused by power fluctuations. An empirical absorption correction was made on the basis of the average of three ψ-scans. A careful examination of the data set did not provide any additional absence conditions. The 3-fold redundant data ($I > 0$) were averaged for the $R\bar{3}$ Laue class with a relatively low R_{av} value (2.1%), in part because of the high percentage of observed data. Trial positions from the parent compound were assumed and successfully refined. A difference Fourier map revealed a residue peak of about 5 e/Å^3 at the center of the cluster after the heavier atoms had been refined anisotropically. Carbon, the only known interstitial element present in the starting materials, was added at this point and refined.

The occupancies of the cation positions as well as the interstitial site were examined. Both Ba and C were, as expected, fully occupied (Ba 100.2(2)%, C 100(2)%), but the simultaneous refinement of the thermal parameters and occupancy of the nominal K position was troublesome; the B_{iso} value increased from 2.87(6) to 3.85(4) Å^2 while the occupancy boomed to 125.9(5)%, which is structurally impossible. Considering that the initial reaction had a K deficiency and the 12-coordinate site is large enough for Ba, partial substitution of K by Ba was refined with the same positional and thermal parameters. The total charge contributed by the mixed-cation position M (K_x+Ba_y) should be +1 ($x + 2y$) for adherence of the cluster of a 14-e count, and as a consequence, the total occupancy of this position should be <1. Multiplicities of both K and Ba2 were refined independently to give $K_{0.85(9)}Ba_{0.13(3)}$. The validity of this refinement was supported by the improved quality of the entire structural solution. In comparison with the model with only K on the M site, the mixed-cation model reduced the difference Fourier peak around this position from 2.5 to 0.5 e/Å^3, and the standard deviations of all positional and thermal parameters decreased by a factor of 2. Therefore, the composition of the crystal was concluded on the basis of the single-crystal structural analysis to be $M_2BaZr_6Cl_{18}C$ with M = $\sim K_{0.85}Ba_{0.13}$. The final ΔF map was flat to 0.5 e/Å^3.

$CsLaZr_6Cl_{18}Fe$. The crystals were black under reflected light and dark purple under transmitted light and had roughly rodlike shapes. Several crystals examined on the diffractometer belonged to the $R\bar{3}$ structure but seemed to have a twinning problem and exhibited profiles with significant splitting. One with satisfactory peak profiles indexed instead to a primitive hexagonal cell, which could include $P\bar{3}1c$. Axial photographs were normal yet failed to provide any symmetry information, and the program check of supposedly equivalent reflections indicated only $\bar{3}$ symmetry. One hemisphere of data was collected at room temperature, but another check of Laue symmetry at the end of this with the refined cell parameters and orientation matrix did not yield the expected Laue symmetry $\bar{3}1m$ of the supposed parent compound $CsLuNb_6Cl_{18}$.

The ability of the RIGAKU software package to provide symmetry information through axial photographs and the above check of symmetry is limited, and careful analysis of the data clearly revealed the presence of c glides along the $\vec{a}$, $\vec{b}$, and $\vec{a} + \vec{b}$ directions ($hh2\bar{h}l$, $l = 2n$). The possible space groups were thus limited to $P\bar{3}1c$ and $P31c$, making it almost certain that the crystal was isostructural with $CsLuNb_6Cl_{18}$. An empirical absorption correction applied on the basis of three ψ-scan measurements resulted in a rather high R_{av} (8.9%) for the 6-fold redundant data, probably because of a rather low signal:noise ratio and the larger uncertainty of the weaker reflections. Successive isotropic and then anisotropic refinements using $CsLuNb_6Cl_{18}$ as a model were successful, and a ΔF synthesis map clearly indicated a large peak at the center of the cluster (~20 e/Å^3), after which an Fe atom was added to the atom list. Simultaneous refinement of the thermal parameters and occupancies of both cation positions showed they were fully occupied (La 101.2(4)%, Cs 103.0(5)%), whereas the same procedure led to only 81.0(6)% occupancy for Fe. A similar phenomenon has occasionally been noticed for other cluster phases with either main-group or transition-metal interstitials.[3,16,17] However, no cluster phases with partially filled interstitial positions have been proven to exist in these systems (except for H). In addition, reducing the amount of the interstitial element provided in the synthesis generally leads to a distinctly lower yield of the cluster phase. A true structural defect at the interstitial site seems unreasonable for this type of cluster, and so such a result has been attributed to systematic errors at this high-symmetry position ($\bar{3}$). In this case, the refinement of the occupancy of Fe did not significantly improve the quality of the overall solution either, and a secondary extinction coefficient was not significant. All the atom positions were fixed at 100% in the final step of the refinement, corresponding to the formula $CsLaZr_6Cl_{18}Fe$.

(16) Zhang, J.; Corbett, J. D. *J. Less-Common Met.* **1989**, *156*, 49.

(17) Smith, J. D.; Corbett, J. D. *J. Am. Chem. Soc.* **1985**, *107*, 5704.

The final difference Fourier map was essentially flat except for 2 e/Å^3 residues in the center of the rings of six chlorine atoms above and below the Cs atoms and a negative peak of 3 e/Å^3 at Fe. Other important data collection and refinement parameters are listed in Table II. Structure factor data are available from J.D.C.

Results and Discussion

$M_xM'Zr_6Cl_{18}Z$. The new phases discovered are listed in Table I with the lattice constants refined from Guinier powder diffraction data for either the $K_2Zr_7Cl_{18}H$ ($R\bar{3}$) or the $CsLuNb_6Cl_{18}$ structure ($P\bar{3}1c$) types or both. All of the clusters in these apparently contain the ideal 14 or 18 cluster-based electrons.

The variety of interstitial atoms possible in the 6–18 clusters in the $R\bar{3}$ type structure now includes H, Be, B, C, Mn, and Fe. An N-centered example like $KBaZr_6Cl_{18}N$ has not been studied. At the other extreme, Cr- or V-centered Zr_6Cl_{12} clusters do not form, and Co gives only $Zr_6Cl_{15}Co$[3] in reactions loaded to make $LaZr_6Cl_{18}Co$ or $KBaZr_6Cl_{18}Co$. In the new $R\bar{3}$ examples with Z = B or C, the 12-coordinate M position may contain one of the larger alkali metals K, Rb, or Cs, but Na and Li are too small. A 50% occupancy of the single M position can also be forced by the choices of M, M′, and Z through cluster electron count regularities, as verified for $MLaZr_6Cl_{18}Z$ with M = K, Rb, Cs and Z = C, Fe. Variation of M:Zr ratios in the starting materials in these syntheses did not cause any changes in the lattice constants of the cluster products and gave reduced yields away from M:Zr = 1:6. However, the desired $R\bar{3}$ $MLaZr_6Cl_{18}Z$ products for M = Rb, Cs were never obtained free of contamination by the $P\bar{3}1c$ polymorphs although the latter can be obtained as single phases. In addition to the three examples listed in Table I, the $R\bar{3}$ versions of $RbLaZr_6Cl_{18}Fe$ and $CsLaZr_6Cl_{18}C$ were recognized in mixtures with the $P\bar{3}1c$ structure but never in amounts sufficient to refine lattice constants well (≤10 lines). ($RbLaZr_6Cl_{18}C$ was not studied.) Although ternary RNb_6Cl_{18} phases are known (R = rare-earth element) in the $R\bar{3}$ structure,[13] no similar compounds with empty M positions have been observed with zirconium clusters, even with suitable Z, suggesting a significant contribution of the countercation M to the stability of the latter.

A large variety of cations can occupy the six-coordinate M′ position in the $R\bar{3}$ $M^1_{1,2}M'Zr_6Cl_{18}Z$ systems, namely, an alkaline-earth or rare-earth metal or Zr itself in $K_2Zr_7Cl_{18}H$ and $K_2Zr_7Cl_{18}Be$. The higher charged M′ cations appear essential to achieve the optimal cluster electron counts and to provide strong interactions within the cluster network in the absence of direct intercluster connections. On the other hand, the $P\bar{3}1c$ version of $MM'Zr_6Cl_{18}Z$ seems to be more restricted regarding composition. The cluster electron count requirements, a fixed M:cluster ratio, and an apparent need for $M' = R^{3+}$ limit the interstitial to C and Fe. Substitution of an alkaline-earth metal for M′ or a change of the interstitial to B or Mn requires an increase in the alkali metal:cluster ratio to 2, and this affords only the $R\bar{3}$ phase. As mentioned previously, there is also a restriction on the size of M, namely, larger than potassium in either zirconium (with M′ = La) or niobium systems;[13] otherwise, the $R\bar{3}$ structure is formed with the M site 50% occupied.

The lattice constants listed in Table I reveal how the dimensions of the $R\bar{3}$ phases are sensitive to the choice of interstitial atom, countercation, and the occupancy of the M sites. This is different from the case of the niobium analogues, where the cell parameters depend significantly on the size of the rare-earth element in the M′ position but are rather insensitive to the size of M.[13] This difference may be attributed largely to the fact that most of the isostructural niobium clusters (except $M_2EuNb_6Cl_{18}$) exist as $MRNb_6Cl_{18}$ compositions with the M positions only half-occupied so that interactions between M and the structure framework are less pronounced. The volume changes induced by the choice of structure type are also distinctive. For instance, the $R\bar{3}$ version of $CsLaZr_6Cl_{18}Fe$ has a formula volume that is 8.0(2) Å^3 (1.1%) larger than the $P\bar{3}1c$ type, indicating a higher space-filling efficiency in the latter (see structure descriptions).

Conversion between the $R\bar{3}$ and $P\bar{3}1c$ Types. One interesting phenomenon observed in this study was that reactions loaded to produce $CsLaZr_6Cl_{18}Z$ (Z = C, Fe) and $RbLaZr_6Cl_{18}Fe$ always yielded a mixture of the $R\bar{3}$ and $P\bar{3}1c$ types under typical experimental conditions (800–850 °C, 15 days). The nature of this equilibrium or transition was explored for $CsLaZr_6Cl_{18}Fe$.

The stoichiometries of the reactions were first varied since the $R\bar{3}$ phase may contain up to two M atoms per cluster. However, an increased M content neither lowered the relative yield of the $P\bar{3}1c$ phase nor changed the lattice constants of either phase, indicating that the stoichiometries are to a large extent fixed and controlled by the electron count via Z. The influence of temperature was also studied. Since the two space groups do not have a group–subgroup relation, the possibility of a second-order phase transition was eliminated, even though the two phases seemingly coexisted over a temperature range as wide as 600–900 °C in several reactions. For a first-order phase transition, two phases of the same composition may be at equilibrium only at a sharply defined temperature.

The effect of time was more revealing. Among two reactions with the same stoichiometry, reaction temperature, and time (1–2 weeks), the one that had been air-quenched had the higher content of the $R\bar{3}$ phase compared to that which had been subsequently annealed at a lower temperature or slowly cooled to 400 °C after the reaction period. However, a conclusion that the product ratio was temperature dependent or that lower temperature favored the $P\bar{3}1c$ phase would overlook the fact that the quenched reactions obviously also had shorter total reaction periods. Another pair of like reactions were therefore carried out at 700 or 900 °C for 70 days, supposedly sufficient for each system to achieve equilibrium, and both were quenched. The result of this experiment was at the time surprising as both reactions yielded a single $P\bar{3}1c$ product. Thus, our revised interpretation is that the $R\bar{3}$ phase is metastable and occurs along the conversion of starting materials into the final $P\bar{3}1c$ product. The transition from the $R\bar{3}$ phase to the thermodynamically more stable (and more compact) $P\bar{3}1c$ form of $CsLaZr_6Cl_{18}Fe$ presumably has a high activation barrier and requires a remarkably long reaction time.

Coexistence of $R\bar{3}$ and $P\bar{3}1c$ types has also been observed for $RbRNb_6Cl_{18}$ (R = La, Ce).[13] The former was the principal (but not the sole) product at 600–700 °C, whereas the proportion of the $P\bar{3}1c$ type increased with temperature over 700–800 °C but without evidence of a transition temperature. Only the $P\bar{3}1c$ form was obtained at 800 °C, but this conversion could not be reversed at 700 °C.[18] The conclusion was that the $R\bar{3}$ phase was more stable at lower temperatures even though a true equilibrium could not be demonstrated.

Clearly a kinetic interpretation will fit both systems. The $RbRNb_6Cl_{18}$ reactions are intrinsically faster but they do not reach equilibrium below 800 °C in the typical reaction periods (24 h), giving the impression of a more stable $R\bar{3}$ structure at lower temperatures. The fact that dimorphism occurs for $RbRNb_6Cl_{18}$, whereas the $CsRNb_6Cl_{18}$ series exhibits only the $P\bar{3}1c$ phase, probably originates with the relatively smaller cluster core (d(Nb–Nb) = 2.91–2.92 Å in $CsLuNb_6Cl_{18}$). This leaves the countercation Cs^+ too large for the $R\bar{3}$ structure relative to the alternate.

Structure Descriptions. The positional and isotropic equivalent thermal parameters and important distances and angles from the two single-crystal analyses are listed in Tables III and IV, respectively.

$(K+Ba)_2BaZr_6Cl_{18}C$. The structure of $(K_{0.85}Ba_{0.13})_2BaZr_6Cl_{18}C$ (=$K_{1.7}Ba_{1.3}Zr_6Cl_{18}C$) is depicted in a [110] section in Figure 1. The general network derives from $(Zr_6Cl_{12}C)Cl_6^a$ clusters,

(18) Ihmaine, S., Thesis, University of Rennes, 1988; p 64.

Table III. Positional Parameters for $M_2BaZr_6Cl_{18}C$[a] and $CsLaZr_6Cl_{18}Fe$

	x	y	z	B_{eq},[a] Å^2
		$M_2BaZr_6Cl_{18}C$		
Zr	0.02423(2)	0.20502(2)	0.048597(7)	1.06(1)
Cl1	0.22490(7)	0.19787(7)	0.10920(2)	1.76(3)
Cl2	0.42599(6)	0.17339(7)	0.00019(2)	1.74(3)
Cl3	0.04060(8)	0.43723(7)	0.10405(2)	2.11(3)
Ba	0	0	$^1/_2$	1.85(2)
M[b]	0	0	0.22080(5)	2.87(6)
C	0	0	0	1.0(2)
		$CsLaZr_6Cl_{18}Fe$		
Zr	0.22047(6)	0.04109(7)	0.07524(3)	1.17(2)
Cl1	0.1919(2)	0.2344(2)	0.1610(1)	1.81(5)
Cl2	0.1494(2)	0.4250(2)	0.0007(1)	1.71(5)
Cl3	0.4575(2)	0.0744(2)	0.1623(1)	2.21(6)
La	$^2/_3$	$^1/_3$	$^1/_4$	1.43(3)
Cs	$^1/_3$	$^2/_3$	$^1/_4$	7.8(1)
Fe	0	0	0	1.64(5)

[a] $B_{eq} = (8\pi^2/3)\sum_i\sum_j U_{ij}a_i^*a_j^*\bar{a}_i\bar{a}_j$. [b] M = $K_{0.85(9)}Ba_{0.13(3)}$.

Table IV. Important Distances (Å) and Angles (deg) in $M_2BaZr_6Cl_{18}C$[a] and $CsLaZr_6Cl_{18}Fe$

Distances

$M_2BaZr_6Cl_{18}C$			$CsLaZr_6Cl_{18}Fe$		
Zr–C	×6	2.2757(2)	Zr–Fe	×6	2.3943(5)
Zr–Zr	×6	3.2118(3)	Zr–Zr	×6	3.391(1)
	×6	3.2248(3)		×6	3.3813(9)
$\bar{d}$		3.2183	$\bar{d}$		3.386
Zr–Cl^{i}1	×6	2.5460(6)	Zr–Cl^{i}1	×6	2.557(2)
	×6	2.5509(6)		×6	2.568(2)
Zr–Cl^{i}2	×6	2.5237(5)	Zr–Cl^{i}2	×6	2.545(2)
	×6	2.5251(6)		×6	2.549(2)
$\bar{d}$		2.5364	$\bar{d}$		2.555
Zr–Cl^{a}3	×6	2.6207(5)	Zr–Cl^{a}3	×6	2.671(2)
Ba–Cl3	×6	3.0651(6)	La–Cl3	×6	2.801(2)
M–Cl1	×3	3.632(1)	Cs–Cl1	×6	4.025(2)
M–Cl1	×3	3.7624(6)	Cs–Cl3	×6	3.842(2)
M–Cl2	×3	3.646(1)	$\bar{d}$		3.934(3)
M–Cl3	×3	3.2160(6)			
$\bar{d}$		3.564			

Angles

$M_2BaZr_6Cl_{18}C$		$CsLaZr_6Cl_{18}Fe$	
Zr–Cl1–Zr	78.50(2)	Zr–Cl1–Zr1	82.85(5)
Zr–Cl2–Zr	79.01(2)	Zr–Cl2–Zr1	83.19(5)
C–Zr–Cl3	177.85(2)	Fe–Zr–Cl3	177.39(6)
Zr–Cl3–Ba	124.60(2)	Zr–Cl3–La	129.87(6)
Cl3–Ba–Cl3	180	Cl3–La–Cl3	162.94(6)
	92.64(2)		90.34(6)
	87.36(2)		89.99(7)

[a] M = $K_{0.85(9)}Ba_{0.13(3)}$.

the Cl^a atoms of which are also bonded to Ba^{2+} (M′) ions situated between every third pair of chlorine layers. The M (K+Ba) ions are substituents within two-thirds of these chlorine layers with the centered carbon atom occurring in the third layer. The $[Zr_6Cl_{18}C]^{4-}$ cluster has S_6 point symmetry, and the Zr_6 metal core deviates from an ideal octahedron only through a slight trigonal compression, the two types of Zr–Zr distances differing by only 0.013 Å (43σ, 0.4%). This is much less than the 0.046 Å observed in the parent compound, $K_2Zr_7Cl_{18}(H)$,[7] a 13-e cluster phase where the M′ cation Zr^{4+} has a stronger field. The Zr–C and average Zr–Zr distances fall into the range expected for 14-electron carbide clusters and so does the average Zr–Cl^i distance.[1,5] The difference between the two types of Zr–Cl^i bonds follows the same pattern observed for the parent compound, the shorter Zr–Cl2 reflecting a lower coordination number of Cl2 [2(Zr) + 1(K)] than of Cl1 [2(Zr) + 2(K)]. The Zr–Cl3^a distance is shorter than the intrinsically longer bridging Zr–Cl^{a-a} in many

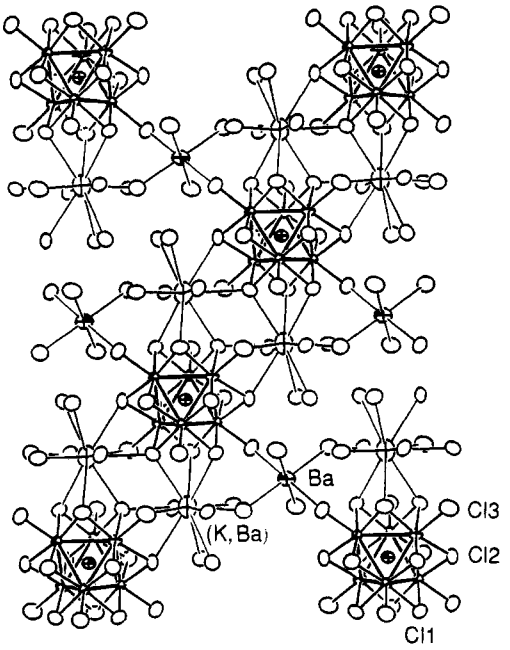

Figure 1. [110] projection of the structure of $(K+Ba)_2BaZr_6Cl_{18}C$ ($R\bar{3}$). (90% probability ellipsoids are used in all figures.)

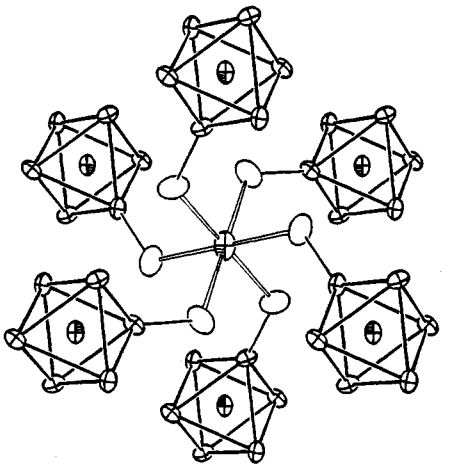

Figure 2. Coordination environment about Ba (M′) in $(K+Ba)_2BaZr_6Cl_{18}C$ and the surrounding cluster units. (Only the bridging Cl3^a anions are shown in the latter.) The $BaCl_6^{2-}$ group has D_{3d} symmetry with the 3-fold axis perpendicular to the plane of the paper.

carbon-centered clusters or the Zr–Cl^a in $K_2Zr_7Cl_{18}H$ where all Cl^a have a second Zr neighbor rather than Ba.

Ba^{2+} occupies the six-coordinate M′ position. The local symmetry is D_{3d} (Figure 2), distorted away from a perfect octahedron through a trigonal compression (d(Cl3–Cl3) = 4.538 and 4.134 Å). The Ba–Cl distance, 3.0651 Å, is less than the sum of crystal radii (3.16 Å[19]) and is the shortest observed in Ba-containing cluster compounds, namely $Ba_2Zr_6Cl_{17}B$[16] and $Ba_3Zr_6Cl_{18}Be$.[14] This doubtlessly originates with the presence of six more basic, two-coordinate Cl^a neighbors from the clusters here, whereas Ba in the other phases has either shared Cl^a or Cl^i nearest neighbors. Although the size, field, and chemical properties of Ba^{2+} are quite different from those of Zr^{4+} in $K_2Zr_6Cl_{18}H$ and R^{3+} in the niobium compounds, it performs the same function as do the other two cations, i.e., linking six clusters together into a structure network.

The M position is 12-coordinate (Figure 3) and statistically occupied by 0.85(9) K and 0.13(3) Ba. This result is reasonable as well (within rather large uncertainties); the sum is less than 1, and the effective charge at this position, 1.1(1), is in good

(19) Shannon, R. P. *Acta Crystallogr.* **1976**, *A32*, 751.

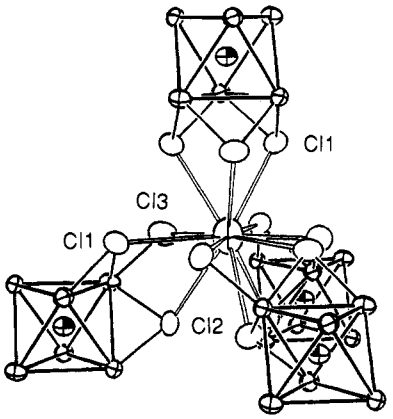

Figure 3. The mixed-cation site in $(K+Ba)_2BaZr_6Cl_{18}C$. The MCl_{12} fragment has C_3 symmetry (3-fold axis vertical) and is generated by four cluster units (other Cl omitted).

agreement with the expectation of 1.0 for a cluster with the optimal 14-e count. A similar position is occupied by Ba2 in the superstructure $Ba_3Zr_6Cl_{18}Be$ ($R\bar{3}c$). Although the present site has only C_3 symmetry, the coordination polyhedron is rather regular: three short (Cl^a) and three long distances around the waist with six other chlorine neighbors in an intermediate range at the top and the bottom. The M site is a member of the close-packed layers dominated by Cl atoms (Figure 1). If the clusters are instead considered as the basic structural elements, the mixed cations are in tetrahedral vacancies defined by the clusters; one cluster contributes three $Cl1^i$ while each of the other three provides one each $Cl1^i$, $Cl2^i$, and $Cl3^a$. The M^+ are displaced, apparently by interactions with the closest zirconium in the cluster cores, so as to be 0.16 Å off the center of the close-packed layers containing Cl1 and Cl3 (upward in Figure 3). The striking difference of over 0.4 Å in M–Cl^i vs M–Cl^a distances once again originates with different field strengths or basicities of the two types of halide.[4,5] The $Cl3^a$ with neighbors of 1(Zr) + 1(Ba) + 1(M) have M–Cl^a distances well below the sum of the corresponding crystal radii average while both Cl^i with 2(Zr) + (Ba) + 1(M) neighbors exhibit M–Cl^i distances 0.24 Å above this value. In contrast, the order of the K–Cl^a and the K–Cl^i distances in the parent salt, $K_2ZrZr_6Cl_{18}H$, is reversed and the difference between them is <0.2 Å, because the countercation Zr^{4+} (vice Ba^{2+}) with short d(Zr–Cl^a) makes the Cl^i and Cl^a atoms more similar.

The function of M is basically to fill space and provide electrons. Although its structural and electronic contributions are essential to the stabilization of this phase, the M–Cl interactions are less important relative to other types. This is reflected by the rather significant deviation of the average M–Cl distance from the sum of the crystal radii as well as by its large thermal ellipsoid somewhat elongated along $\vec{c}$ (Figure 3). As also observed in the parent compound, the oversized M position and the smaller distance between the M′ cation to its neighboring Cl's seem to be common characteristics of this structure and direct indications of the difference functions of the two cationic structural elements. The M site may be 50% occupied with a suitable choice of M′ and Z, e.g., in $KLaZr_6Cl_{18}C$ and $KLuNb_6Cl_{18}$.[12,13] It may also be left empty in the presence of a small rare-earth metal as M′ and a less reduced niobium cluster, as in $LuNb_6Cl_{18}$,[12] but this could not be achieved for zirconium examples.

The close-packed layered representation of this structure has been clearly stated for the parent compound;[7] nine layers along $\vec{c}$ in the sequence (...ABABCBCAC...) or $(chh)_3$ (Figure 1). The cross section of each layer perpendicular to $\vec{c}$ contains seven close-packing positions (7 × 9 in each unit cell) that are occupied by either Cl, C, or K atoms [3(2K + 18Cl + C)] with no vacancies. The layers are approximately equally spaced, but the three layers around the common cluster core are pulled closer to each other (2.88 Å) by Zr atoms while the layers having only Ba^{2+} between

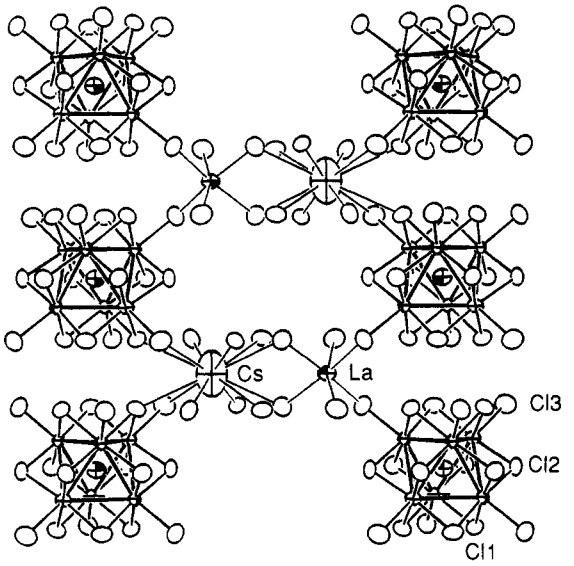

Figure 4. [110] projection of $CsLaZr_6Cl_{18}Fe$ ($P\bar{3}1c$, $\vec{c}$ vertical). The c glide is perpendicular to the plane of the paper and passes through the center of each vertical column of clusters.

them are further apart (3.23 Å). The close (Cl1···Cl3) separation, 3.3968(8) Å, probably results from their connection to common Zr and M atoms.

$CsLaZr_6Cl_{18}Fe$. A [110] section is shown in Figure 4. In this structure type both the Cs (M) and La^{3+} (M′) ions are bound *between* layers, the latter again only to formal Cl^a atoms on the clusters. The Cl2 layers are continuous through the center of the figure, but some are members of clusters that lie outside of this section and are therefore not shown (compare Figure 1).

The 18-e cluster unit $[Zr_6Cl_{18}Fe]^{4-}$ has S_6 point symmetry, with a trigonal compression of the octahedral cluster core that is almost negligible (0.0097 Å, 7σ). The average Zr–Fe distance, 2.394 Å (as well as the geometrically related Zr–Zr value), is the shortest among those known in other 18-e-Fe-centered cluster compounds, which average very close to 2.423 Å in $Zr_6Cl_{14}Fe$, $LiZr_6Cl_{15}Fe$, and $KZr_6Cl_{15}Fe$.[3,20] This is a good example of the secondary effects of cation interactions on exo chlorine,[5] in this case between the Cl^a atom at each vertex and the higher field La^{3+}. Iron and Cl^a are trans to one another and compete for the same σ orbitals on zirconium. The stronger La^{3+} interaction elongates Zr–Cl^a, making it comparable to the intrinsically longer Zr–Cl^{a-a} bonds in the three comparisons above, which, in a complementary manner, results in a shorter Zr–Fe separation.

The average Zr–Cl^i distance is the upper limit for Fe-centered clusters and a result of the higher coordination numbers of these Cl^i atoms. As expected, the $Cl1^i$ atom with a higher coordination number [2(Zr) + 1(Cs)] has longer Zr–Cl^i distances than Cl2 [2(Zr)]. Comparison of the d(Zr–Cl^a) in this compound with those in other $M_xM'Zr_6Cl_{18}Z$ phases clearly shows that this distance increases as the oxidation state of M′ increases and the Cl^a–M′ interactions become stronger [2.619(1) Å with Ba^{2+} in $(K+Ba)_2BaZr_6Cl_{18}C$; 2.6711(2) Å to La^{3+} here; 2.770(2) Å to Zr^{4+} in $K_2Zr_7Cl_{18}H$[7]].

The six-coordinate La^{3+} in $CsLaZr_6Cl_{18}Fe$ still connects to six cluster units through Cl^a, as in the $R\bar{3}$ structure, yet the coordination polyhedron of clusters depicted in Figure 5 is no longer a trigonal antiprism (compare Figure 2). A twist of the top and bottom triangles of clusters (and their layers) around the 3-fold axis has destroyed the inversion center of the antiprism and reduced the point symmetry to D_3. The largest Cl3–La–Cl3 angle is now 162.92(6)° instead of the ideal 180° in the $R\bar{3}$ form; however, the angle at Cl^a differs by only about 5° and that for Fe–Zr–Cl^a remains almost the same. Thus, the network changes

(20) Zhang, J.; Corbett, J. D. Unpublished research.

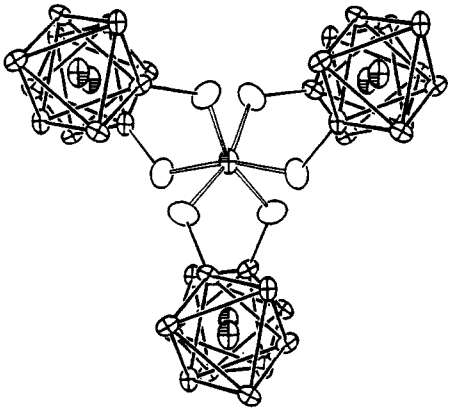

Figure 5. The La position (D_3 symmetry) in $CsLaZr_6Cl_{18}Fe$ and the cluster units around it as viewed along the principal axis.

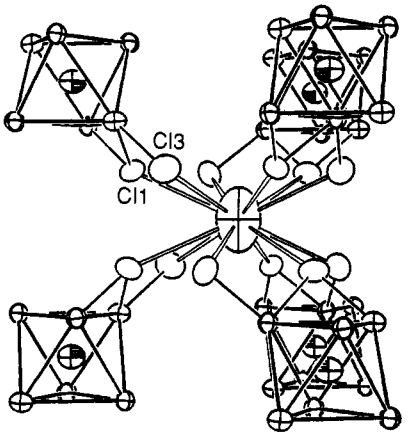

Figure 6. The Cs position in $CsLaZr_6Cl_{18}Fe$ (D_3 symmetry with the 3-fold axis vertical).

on going from the $R\bar{3}$ to the $P\bar{3}1c$ type primarily involve modifications of the M′ (and M) positions, leaving the cluster units intact and the cluster interconnections preserved.

Contrary to the foregoing, the coordination environment of M in the $P\bar{3}1c$ type is completely different. Although the coordination number is still 12, the larger Cs atoms do not occupy positions within the close-packed layers; instead, they now lie between chlorine layers. Each M atom now has two 6-rings of $Cl1^i$ and $Cl3^a$ above and below it in its first coordination sphere, with D_3 point symmetry for the MCl_{12} group (Figure 6). The average Cs–Cl distance is over 0.2 Å greater than the sum of the crystal radii (CN12: 3.69 Å[19]), mainly because the structure framework does not allow the anions to arrange around Cs^+ freely. The two Cl_6 rings have diameters of 7.27 Å, leaving large openings above and below the Cs atom, and two more distant triangular fragments of Cl2 atoms at 5.03 Å (not shown) complete the coordination along the $\vec{c}$ axis. The size as well as shape of the thermal ellipsoid clearly reflects the size and anisotropy of this Cs site.

Interconversion. As the structure of $MM'Zr_6Cl_{18}Fe$ transforms from $R\bar{3}$ to $P\bar{3}1c$, the close-packed layers are also changed. There are six close-packed layers perpendicular to $\vec{c}$ in each unit cell, and each cross section still contains seven close-packed positions (7×6 per cell). Part of these positions are occupied by Cl atoms and Fe [2(18Cl + Fe) per cell], but four sites located above and below each Cs atom become empty. Three of the six layers located around the clusters centered at $z = {}^1/_2$ do not overlap in projection with any layer around the clusters near $z = 0$ (Figure 4). This is caused by the twisting of the cluster units around the 3-fold axis passing through La (Figure 5), which results in a lateral misplacement by about 10° of the two sets of the close-packed layers now related by the c glide. As a result, the layer sequence becomes (...CABC′A′B′...) where the prime denotes the 10° displacement. The spacing between the layers follows the same pattern (2.963, 3.236 Å) as in $K_2BaZr_6Cl_{18}C$, except the cluster expansion caused by the larger Fe pushes the layers around the same cluster slightly further apart. The closest chlorine neighbors in this structure, Cl1···Cl3 (3.509(2) Å), share common Zr and Cs atoms.

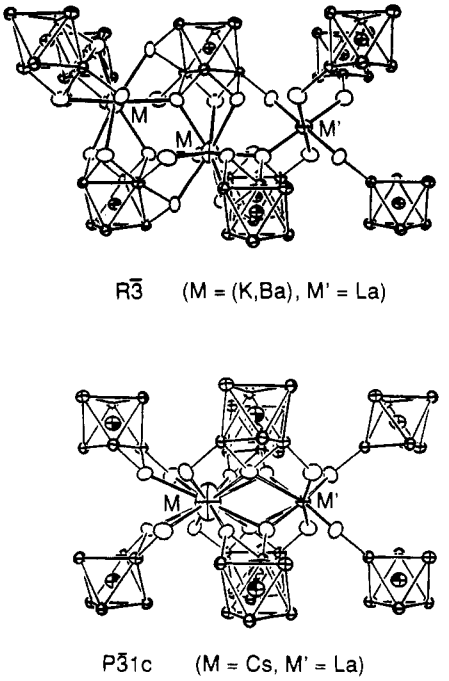

Figure 7. Structural relationship between of $(K+Ba)_2BaZr_6Cl_{18}C$ ($K_2ZrCl_6{\cdot}Zr_6Cl_{12}H$-type, $R\bar{3}$) and $CsLaZr_6Cl_{18}Fe$ ($CsLuNb_6Cl_{18}$-type, $P\bar{3}1c$).

Relationships among Cluster Structures. The three 6–18 structures $(K+Ba)_2BaZr_6Cl_{18}C$, $CsLaZr_6Cl_{18}Fe$, and $Ba_3Zr_6Cl_{18}Be$, are closely related. All are constructed of isolated $Zr_6Cl_{18}Z$ units linked via the countercation M′ and can be represented by the general formula $M_xM'Zr_6Cl_{18}Z$. A second countercation M fills the space left by these two structural elements and, at the same time, fulfills electronic requirements of the clusters. On the other hand, these structures are significantly different in terms of cluster packing and the coordination environment of the countercation positions. The structure variations come about from modifications of the M countercation sites. The coordination polyhedra of the countercations M are not directly involved in the main structure network and are thus more flexible and more sensitive to the changes in its occupancy, size, and charge.

The structure of $CsLaZr_6Cl_{18}Fe$ ($CsLuNb_6Cl_{18}$ type[8]) can be derived from that of $(K+Ba)_2BaZr_6Cl_{18}C$ ($K_2ZrCl_6{\cdot}Zr_6Cl_{12}H$ type[7]) through a twist of the cluster layers in the latter so as to merge two adjacent M sites. The cause of this modification is the tendency for a large M cation (Rb, Cs) to occupy one large vacancy rather than to randomly distribute over two smaller, half-occupied positions. The entire structure responds to this adjustment of the M site with a three-dimensional framework and high efficiency of space filling. Figure 7 shows that while the two nearby M atoms can move toward each other and line up along the $\vec{c}$ direction so as to become one, a rearrangement of their Cl atom neighbors is required. This is accomplished by rotation of the two cluster layers against one another, which twists the coordination polyhedron of the other countercation as well. This structural transition from the $R\bar{3}$ type to the $P\bar{3}1c$ type reduces the M per cluster ratio from 2 to 1, distorts the geometry of the MCl_6 group from trigonal antiprismatic to twisted trigonal prismatic, and changes the cluster packing sequence from (...ABC...) to (...AA...).

The charge of the countercation M is another source of structural modifications. For the parent structure types discussed

above, the M position is occupied mainly by alkali metals, regardless of size or occupancy. When the field strength of the cation in this position is increased by a change to an alkaline-earth metal, a superstructure type of this series results, that of $Ba_3Zr_6Cl_{18}Be$ ($R\bar{3}c$).[14] The modifications again appear mainly around the countercation M and involve three Cl layers. These are necessary responses to contraction of the coordination polyhedra about M (Ba) in order to reduce the repulsions between Cl atoms that come closer. In contrast to the first structural change described above, the close-packed cluster array of the $R\bar{3}$ form is preserved in $Ba_3Zr_6Cl_{18}Be$. The Cl atoms that belong to different cluster layers (Cl1′) have a greater degree of freedom to move than do the others that are fixed to a certain extent within the common cluster layers. Although the rotation of the layer with Cl1′ atoms with respect to the other two does not reduce the total number of Cl close contacts around this position, the repulsions are more evenly distributed rather than concentrated on one group of Cl atoms (Cl3) as would happen if the original ($R\bar{3}$) structure were adopted. This is illustrated in Figure 8. This change involves only the rotations of the cluster units with respect to their centers, and therefore most structure features of the double-salt structure are preserved, including the packing sequence of the cluster units and the location and number of M countercations. However, the orientations of the cluster unit in the neighboring layers are no longer the same, and the range of the chlorine close packing is now confined to one cluster layer. The instability thus introduced apparently is overcome by the increased lattice energy that results from the stronger Ba–Cl interactions.

The above examples demonstrate some of the many factors that are responsible for the structure diversities in the centered Zr_6Cl_{18} cluster systems. Contrasting and sometimes more complicated ways in which larger numbers of alkali-metal cations of different sizes may be ordered around $Zr_6Cl_{18}Z$ anions are well illustrated by the structures of $Rb_5Zr_6Cl_{18}B$,[2] $Rb_4Zr_6Cl_{18}C$, and $Li_6Zr_6Cl_{18}H$.[4] The ability of the cluster structures to accommodate a variety of countercations and the specific structural requirements of these cations can lead to many structurally related phenomena, such as the formation of a new structure type, a transition between phases with different

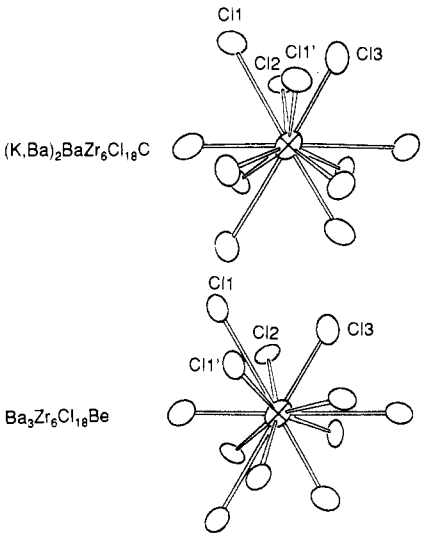

Figure 8. Comparison between the 12-coordinate M positions in $(K+Ba)_2BaZr_6Cl_{18}C$ ($R\bar{3}$) and $Ba_3Zr_6Cl_{18}Be$ ($R\bar{3}c$) with the 3-fold axis perpendicular to the plane of the figure.

structures, or slight modifications that result in a superstructure. Unlike most other structural changes, the relationships among this group of 6–18 structure types are very close. This also implies nearly unlimited possibilities for a diverse structural chemistry of these systems when other factors and variables are taken into consideration and put into effect.

Acknowledgment. Dr. C. Perrin kindly supplied several reaction and structural details prior to their publication. This research was supported by the National Science Foundation, Solid-State Chemistry, via Grants DMR-8318616 and DMR-8902954 and was carried out in the facilities of Ames Laboratory, U.S. Department of Energy.

Supplementary Material Available: Tables of additional crystal and refinement data and anisotropic displacement parameters of $(K+Ba)_2BaZr_6Cl_{18}C$ and $CsLaZr_6Cl_{18}Fe$ (2 pages). Ordering information is given on any current masthead page.